ORIGINAL ARTICLE

Radiosurgical Treatment Planning for Intracranial AVM Based on Images Generated by Principal Component Analysis - A Simulation Study

Osamu Kawaguchi,[1] Yoshiyuki Nyui,[2] Etsuo Kunieda,[1] Satoshi Onozuka,[1] Nobuhiro Tsukamoto,[3] Junichi Fukada,[1] Toshio Ohashi,[1] Subaru Hashimoto,[1] Koichi Ogawa[4] and Atsushi Kubo[1]

[1]*Department of Radiology, Keio University, Tokyo, Japan*
[2]*Department of Radiological science, Faculty of Health sciences, Tokyo Metropolitan University, Tokyo, Japan*
[3]*Department of Radiation Oncology, Saitama Medical University International Medical Center, Saitama, Japan*
[4]*Department of Electronic Informatics, College of Engineering, Hosei University, Tokyo, Japan*

(Received for publication on October 10, 2008)
(Revised for publication on November 5, 2008)
(Accepted for publication on November 13, 2008)

Abstract

***Background*: One of the most important factors in stereotactic radiosurgery (SRS) for intracranial arteriovenous malformation (AVM) is to determine accurate target delineation of the nidus. However, since intracranial AVMs are complicated in structure, it is often difficult to clearly determine the target delineation.**

***Purpose*: To investigate the usefulness of principal component analysis (PCA) on intra-arterial contrast enhanced dynamic CT (IADCT) images as a tool for delineating accurate target volumes for stereotactic radiosurgery of AVMs.**

***Materials and Methods*: IADCT and intravenous contrast-enhanced CT (IVCT) were used to examine 4 randomly selected cases of AVM. PCA images were generated from the IADCT data. The first component images were considered feeding artery predominant, the second component images were considered draining vein predominant, and the third component images were considered background. Target delineations were first carried out from IVCT, and then again while referring to the first and second components of the PCA images. Dose calculation simulations for radiosurgical treatment plans with IVCT and PCA images were performed. Dose volume histograms of the vein areas as well as the target volumes were compared.**

***Results*: In all cases, the calculated target volumes based on IVCT images were larger than those based on PCA images, and the irradiation doses for the vein areas were reduced.**

***Conclusion*: In this study, we simulated radiosurgical treatment planning for intracranial AVM based on PCA images. By using PCA images, the irradiation doses for the vein areas were substantially reduced.** (Keio J Med 58 (1) : 41–49, March 2009)

***Keywords*: radiosurgery, target delineation, treatment planning, intracranial AVM, principal component analysis**

Introduction

An intracranial arteriovenous malformation (AVM) is a native deformed vessel in which the artery and vein directly connect without capillary vessels. The walls of this abnormal nidus often break due to the high hydrodynamic pressure of the arterio-venous shunt. This leads to spasms and hemorrhage, and cerebral AVM is a condition that is considered to be fatal with sudden onset. There have been many studies on the nature of AVMs,

Reprint requests to: Osamu Kawaguchi, M.D, Department of Radiation Oncology, Keio University, 35 Shinanomachi, Shinjuku-ku, Tokyo 160-8582, Japan, Tel: +81-3-3353-1211 ex.62531, Fax: +81- 3-3359-7425, E-mail: kawaguti@rad.med.keio.ac.jp

and Pellettieri *et al*. hypothesized that the increase in size and debatable size-dependent risk of AVM hemorrhage could be attributed to an anatomical entity.[1]

Recently, stereotactic radiosurgery (SRS) has been useful as a treatment method for small AVMs when ordinary surgical methods are too difficult to apply due to the location of the lesion or the patient's status. With SRS, the probability of a cure will increase and the risk of radiation injury will diminish if the target of the beam concentration corresponds to the AVM nidus with minimal irradiation of the surrounding normal tissue.[2,3] In particular, irradiation of draining veins may cause them to collapse before the nidus has been obliterated, leading to higher blood pressure on the nidus wall and eventually resulting in accidental hemorrhage.[4,5] Therefore, in order to minimize such complications, draining veins should be kept outside the irradiation area. To date, target delineation for AVM has been based on magnetic resonance imaging (MRI) and intravenous contrast-enhanced computed tomography (IVCT) images with reference to angiograms. As for three-dimensional (3D) reconstruction of the brain's blood vessels, various methods have been proposed. Yeung *et al*. developed a technique for reconstructing the AVM from multi-directional stereotactic angiograms.[6] This technique is precise, with sub-millimeter accuracy, and is useful for radiosurgical treatment planning. Tanaka *et al*. demonstrated the value of helical CT and CT angiography in evaluating the target for therapeutic planning of cerebral AVM, and compared this with time-of-flight MR angiography and digital subtraction angiography.[7] In addition, Stancanello *et al*. reported a method for registration of CT and 3D angiography for AVM radiosurgery.[8]

Generally, in intracranial AVM feeding arteries, the nidi and draining veins are complicated in their structure, making it very difficult to accurately determine target delineation with conventional methods for radiosurgical treatment planning. Our method used a sequence of dynamic CT images obtained by intra-arterial infusion of contrast medium. To identify the nature of the contrast-enhanced vessels, we used information on blood flow conditions (inflow and outflow) in these structures. That is, the acquired images were analyzed using the principal component analysis (PCA) method.[9] PCA is a well-known technique in the nuclear medicine field for image reconstruction.[10–12] Knuttsson *et al*. applied PCA for whole cerebral blood flow quantification,[13] and Eida *et al*. reported on MR factor analysis for two-dimensional MR dynamic images of benign and malignant salivary gland tumors.[14]

The purpose of this study was to examine the usefulness of the PCA method for delineating accurate target volumes for stereotactic radiosurgery (SRS) of AVMs. Using PCA images, we performed a simulation of SRS treatment planning. In addition, we compared dose volume histograms of the vein area as well as target volumes.

Materials and Methods

Four patients with cerebral AVMs were randomly selected from our radiosurgical database. Case 1 was a 12-year-old female with an intracranial AVM in the left parietal lobe. Case 2 was a 39-year-old male with an intracranial AVM in the left frontal lobe. Case 3 was a 54-year-old male with an intracranial AVM in the right parietal lobe. Case 4 was a 39-year-old female with an intracranial AVM in the right temporal lobe. **Figure 1** shows Case 2 as a representative example using digital subtraction angiography (DSA).

All of the patients were treated by SRS and had previously been studied using intravenous contrast-enhanced helical CT (IVCT), intra-arterial contrast-enhanced dynamic CT (IADCT), and DSA. IVCT examinations were performed using a helical CT scanner (XVision; Toshiba Medical Systems Corp., Tokyo Japan), with contrast media infusion at 2 ml/sec and with a duration of 45 seconds. The slice thickness for IVCT was 2 mm, and reconstruction was performed with a 1-mm slice thickness after scanning. In this way we obtained homogenous contrast-enhanced images of the entire AVM, including the feeding arteries, nidus, and draining veins. The IADCT examinations were performed using another helical CT scanner (Advantx ACT; GE Medical Systems, Milwaukee, WI) and nonionic contrast medium. We used

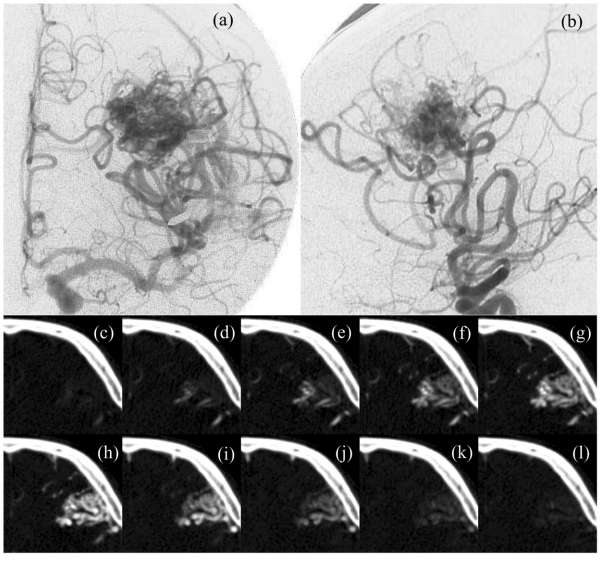

Fig. 1 Posterior-anterior (a) and left-right (b) digital subtraction angiography (DSA) of Case 2.
Intra-arterial dynamic CT (IADCT) images near the center of the nidus in Case 2; (c)-(g) 0.2 sec intervals, (h)-(l) 0.4 sec intervals.

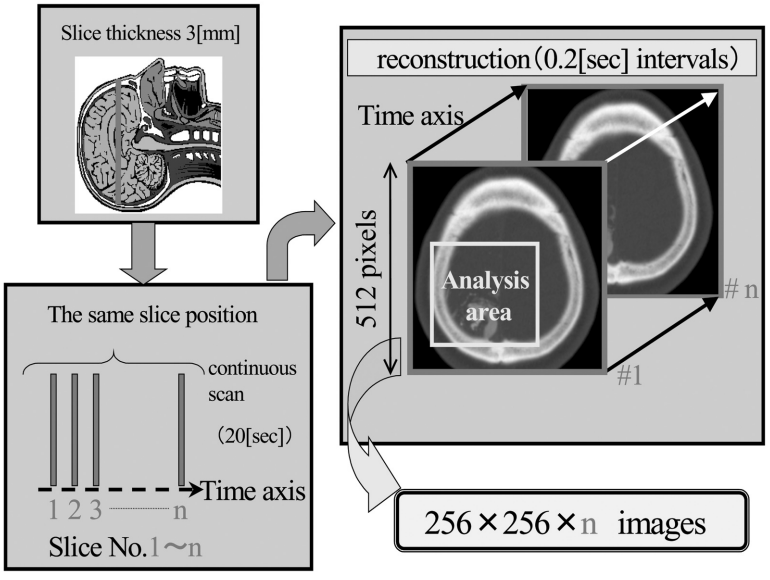

Fig. 2 Schematic representations of data acquisition.

a half concentration (150 mgI/ml) of contrast medium for the IADCT. For each single-shot injection of 1-second duration, 1.5 ml of contrast medium was used. Scanning was continuously performed at a rate of 0.8 sec/rotation for 10 seconds at the same table position using 120 kVp, 60–100mA, and a 3-mm slice thickness. The scan position was then moved 3 mm cranially, and the dynamic scans were repeated to encompass the nidus. **Figure 1** shows a sequence of acquired IADCT images at a position near the center of the nidus in Case 2. A total of 55 images from start to end of contrast enhancement were obtained for each slice position. After the entire examination was completed, sequential images at 0.2 seconds intervals were reconstructed with an image size of 512×512 pixels, and a pixel size of 0.6×0.6 mm^2.

The IADCT images were analyzed using the PCA method and free software (Pixies Micro Edition, ver. 0.99.1; Apteryx, Issy-les-Moulineaux France). For PCA, an orthogonal analysis was first performed, and using the orthogonal analysis results, an oblique analysis was carried out, resulting in component images corresponding to the artery and nidus-predominant component, vein-predominant component, and background component. **Figure 2** provides a schematic illustration of our data acquisition and preprocessing method.

Generally, an increased estimated radiation dose involving DSA, IVCT, and IADCT would be a potential drawback to our proposed method, and the risk-versus-benefit issue would need to be weighed. However, since intracranial AVM is a lethal disease, reducing the risk of hemorrhage is the most important issue. Moreover, secondary risks due to treatment dose are ultimately higher than the risk of radiation exposure from the radiological examinations.

Although our IADCT method for intracranial AVM was approved by the ethical committee of our institute, this study was performed for computational simulation purposes only, using data obtained from IADCT from each patient's clinical treatment.

Treatment Planning

For the purposes of experimentation, SRS treatment planning was carried out virtually using PCA data as well as IVCT data. Based on our standard protocol, AVMs were irradiated with a total marginal dose of 20 Gy given in 1 fraction. The gross target volume (GTV) was determined from the CT data. The clinical target volume (CTV) was considered to be identical to GTV. Margins of 1 mm were added to the CTV in order to create the planning target volume (PTV). Dose deliveries with single isocenter and 10 non-coplanar static beams were carried out. A 6-MV linear accelerator (ML15MV: Mitsubishi Electric Corp., Tokyo, Japan) was used to produce the x-ray beam. A computer-controlled MMLC module (AccuLeaf: Alayna Enterprises Corp., Paris, France) was mounted on the linac gantry-head, and 48 pairs of MMLC leaves, driven by individual motors, were set up on 2 levels with the direction of the 2 levels of leaves perpendicular to each other. The effective leaf thickness of the inner 14 pairs was 2.6 mm, while the thickness of the outer pairs was 5.3 mm at the isocenter.[15]

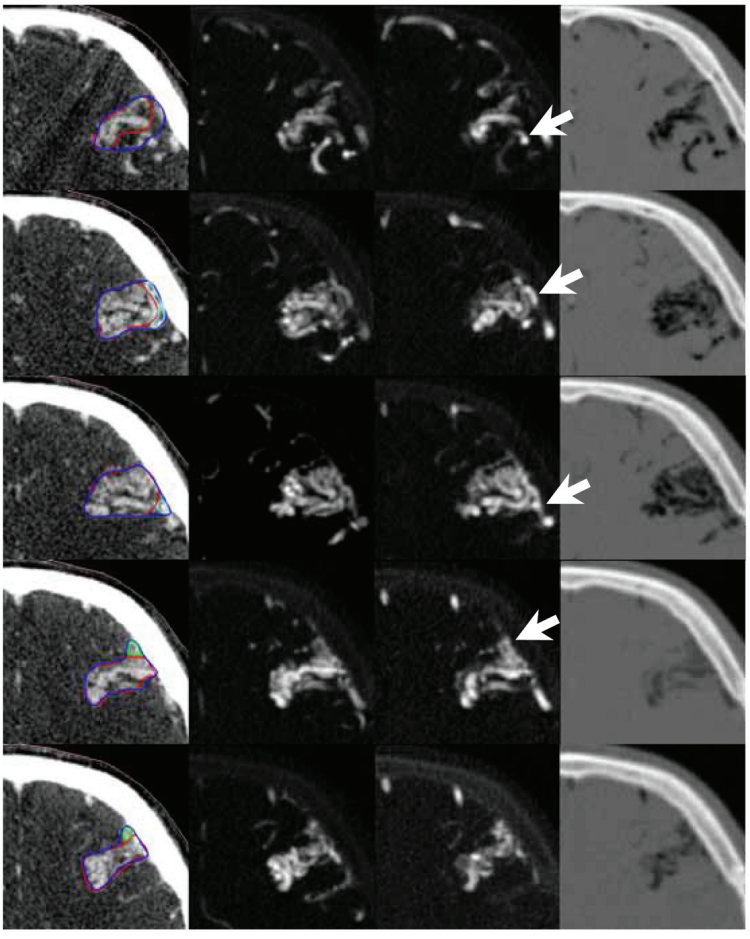

Fig. 3 Intra-venous contrast-enhanced helical computed tomography (IVCT) and principal component analysis (PCA) images for each slice in Case 2.
IVCT with GTV_IV, GTV_PCA, 'vein' ROI delineations and 3 PCA images of IADCT in Case 2. From left to right, IVCT, the first-component, second-component, and third-component images are indicated. From top to bottom, each axial image is indicated at 3 mm intervals. A draining vein (white arrow) is indicated in the second component image. GTV_IV (blue), GTV_PCA (red), 'vein' ROI (sky blue and green) delineations are also indicated.
GTV: Gross target volume

Target delineation

The GTV outline was delineated using IVCT (**Fig. 3**: GTV_IV, blue line) by an individual operator who had not been involved in the study design and who had not seen the PCA images at that time. In order to be used as support information for GTV delineation, DSA and MRI images were allowed as references. Four weeks after the delineation of GTV_IV, the same operator delineated the GTV_PCA outline, referring to the first and second images from the PCA results (**Fig. 3**: red line). In order to evaluate the difference between GTV_IV and GTV_PCA, an experienced radiation oncologist, who had over 10 years experience with radiosurgery planning, very carefully delineated the area of 'vein' regions of interest (ROI) (**Fig. 3**: sky blue and green lines) using all the available data from PCA, IVCT, DSA, and MRI, and considering the connection of the vessels in a 3D manner.

Plan generation

Two SRS plans were generated from the GTV_IV and GTV_PCA individually. Using the micro-multileaf collimator, 10 non-coplanar static beams were simulated with a prescribed dose level of 20 Gy. In generating the IV_plan and PCA_plan, we used the same beam parameters of gantry angles and couch angles as the template. The details of the beam parameters are described in **Table 1**. The dose distributions of the IV_plan and

Table 1 IV plan and PCA plan beam parameters in Case 2.

Case 2 Beam parameters						
Common parameters			IV plan		PCA plan	
Beam No	Couch Angle [deg]	Gantry Angle [deg]	Weight [of 1000]	MU	Weight [of 1000]	MU
1	320	29	90	245	95	257
2	330	340	90	249	85	236
3	338	299	98	311	95	305
4	340	80	114	315	123	335
5	0	46	118	309	106	279
6	0	18	86	228	92	245
7	0	304	94	311	106	351
8	18	54	114	299	102	268
9	53	59	110	289	99	260
10	85	95	86	234	99	270

Table 2 Radiosurgery treatment summary of Cases 1-4.

SRS treatment Results								
Case	1		2		3		4	
Plan name	IV plan	PCA plan	IV plan	PCA plan	IV plan	PCA plan	IV plan	PCA plan
Target Name	GTV_IV	GTV_PCA	GTV_IV	GTV_PCA	GTV_IV	GTV_PCA	GTV_IV	GTV_PCA
Target Volume [mm^3]	6701	5859	5665	4829	8367	7042	3501	2977
Min Dose [cGy]	1494	1548	1269	1458	1297	1138	1454	1472
Max Dose [cGy]	2492	2490	2540	2518	2477	2498	2519	2546
Mean Dose [cGy]	2297	2292	2315	2298	2290	2306	2324	2343
Homogeneity Index	1.67	1.61	2.00	1.73	1.91	2.19	1.73	1.73
Conformity Index	1.44	1.54	1.61	1.53	1.48	1.57	1.6	1.65
Min Dose Index (/PD) [%]	75	77	63	73	65	57	73	74
Max Dose Index (/PD) [%]	125	124	127	126	124	125	126	127

PCA_plan were caliculated by treatment planning system (Accusoft; Alayna Enterprises Corp., Paris, France). These plans were not used for actual treatment, but were merely simulations for the purposes of this study.

Results

Figure 3 shows the IVCT images with GTV_IV, GTV_PCA, 'vein' ROI delineations, and the principal component images of IADCT for Case 2. From left to right, the first-, second-, and third-component IVCT images are shown. The 'vein' ROI was basically in the regions that were included in GTV_IV but were excluded from GTV_PCA.

These principal component images can be considered as follows: the first-component image shows predominantly the arterial and AVM region, the second shows predominantly the venous and AVM region, and the third shows the background activity region. In the first set of images, the feeding artery was detectable as the area that had strong intensity, and this finding was confirmed in DSA and IADCT images that observed the anatomical connection. In the second set of images, the draining vein was similarly detected. In the third set of images, bony structures and embolizing opacities were used for confirmation.

Results of treatment planning and dose calculations

Table 2 summarizes the results of the treatment plans (IV_plan and PCA_plan). GTV_IV is larger than GTV_PCA in all cases (**Fig. 4**). The radiation field for the PCA_plan was smaller than that of the IV_plan. As an example, the field shape of beam number 10 in Case 2 is indicated in **Figure 5**. The maximum dose average for all 4 cases for the IV_plan was 25.07 Gy, and that for the PCA_plan was 25.10 Gy. The dose distributions of the IV_plan and PCA_plan are indicated in the same axi-

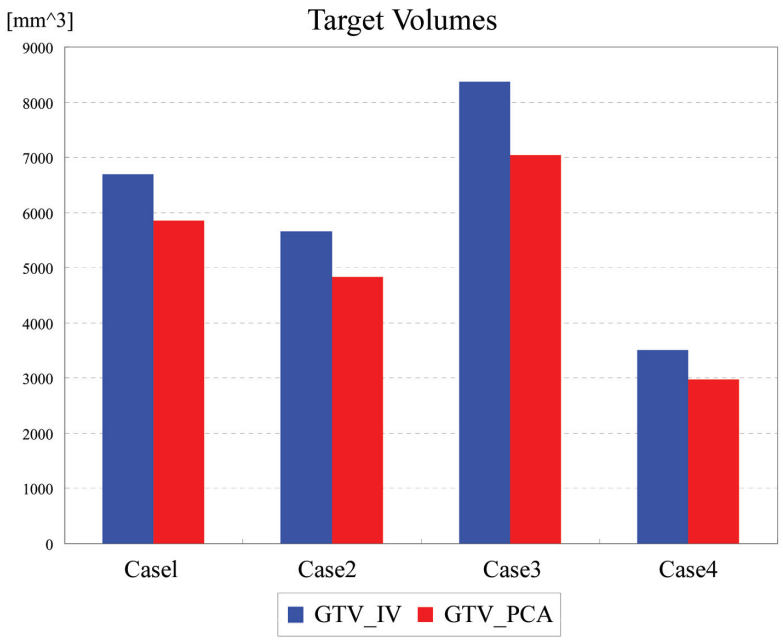

Fig. 4 Target volumes of GTV_IV and GTV_PCA in Cases 1-4.

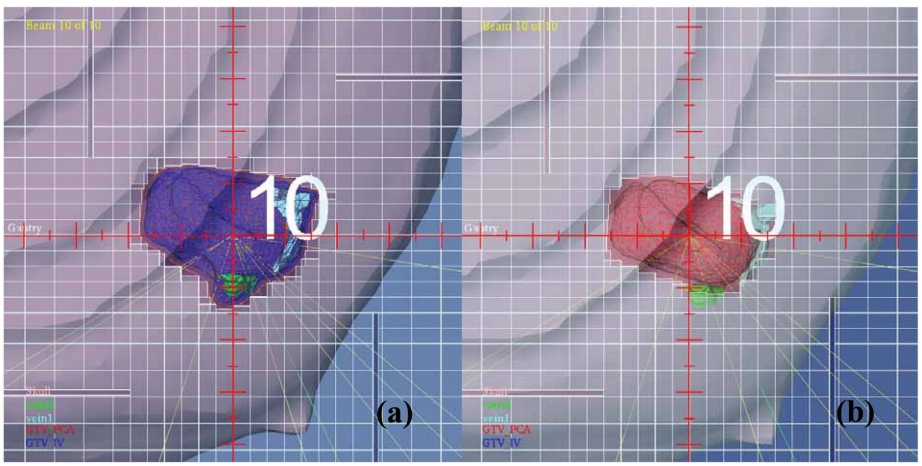

Fig. 5 An example of field shape.
Beam's-eye views of beam number 10 in Case 2 are shown: IV_plan (a), and PCA_plan (b). GTV_IV is shown as a blue, meshed area (a). GTV_PCA is shown as a red, meshed area (b). Organs at risk, 'vein' ROIs are shown as sky blue and green areas. In the PCA_plan, 'vein' ROIs are reduced from the radiation field (b).

al, coronal, and sagittal plane (**Fig. 6**).The dose-volume histograms for the target volumes and 'vein' ROI for each plan in Case 2 are shown in **Figure 7**. The dose-volume histograms for 'vein' ROI are also indicated in **Figure 8**. In the PCA_plan, the mean and minimum dose of 'vein' ROI appeared lower than those in the IV_plan.

Discussion

Many authors have reported that the main issue in radiosurgical treatment of AVMs is definition of the target, and that the target should include the whole of the nidus.[16] On the other hand, it is important to reduce the irradiation volume in order to minimize complications af-

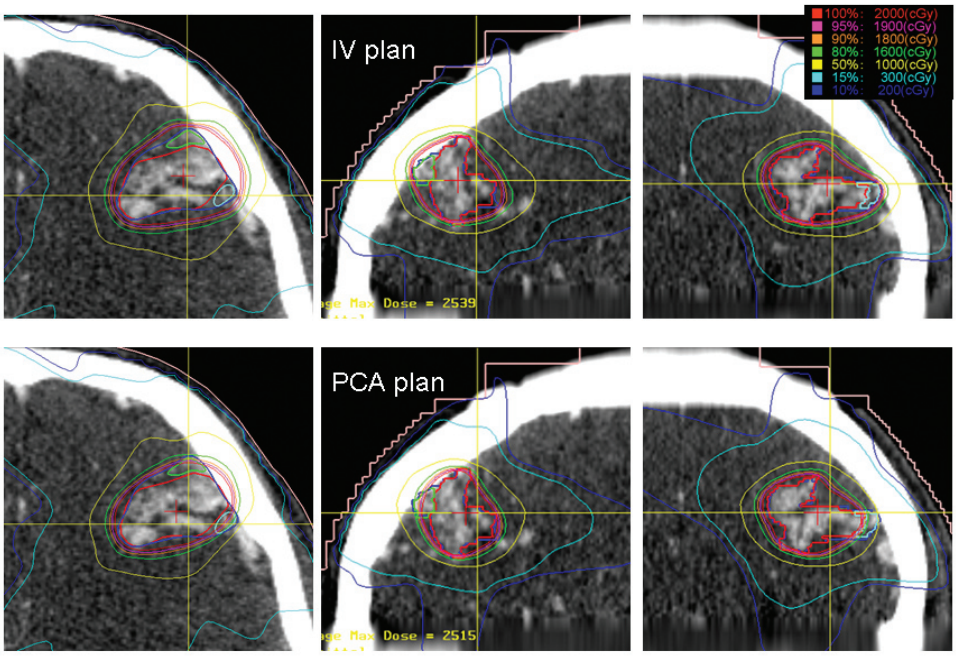

Fig. 6 Dose distributions of the IV_plan and PCA_plan in Case 2.
The IV plan (upper images) and PCA_plan (lower images) are shown. Left to right; axial, sagittal, and coronal images. The red-crossed line shows the position of the isocenter in each plan. The yellow-crossed line shows the position of the sagittal and coronal slices.

ter radiosurgery. In particular, the draining veins should be excluded from the target volume. Conventionally, we have excluded draining veins manually from the target volume on planning CT images by referring to DSA images or MRI images. This operation is very time-consuming and complicated, even when the procedure is potentially feasible. In most cases, it is very difficult and in fact, almost impossible, to identify which points on CT images of each slice correspond to the marked draining vein on DSA images, because the structures are presented two-dimensionally.

IADCT is a useful tool for separating veins from the nidus. However, as an example, in the left image of **Figure 3**, we can identify the shape of the vessels on the whole, but cannot distinguish each vessel component using IVCT images alone. Because an AVM is composed of native deformed vessels where the artery and vein connect directly without capillary vessels, most of the AVM is labyrinthine in structure, with the feeding arteries, nidus, and draining veins. In these cases we cannot remove the draining veins from the target volume because there are overlapping regions of the nidus and the veins. However, with our method, we found that there are some cases in which the draining vein can be excluded from the target volume. In the left image of **Figure 3**, the GTV_IV (blue line) is shown as the target delineation referring only to the IVCT image. Comparing the first-component image and second-component image, we can easily identify the draining vein as part of the second-component image separated from the first-component image. As a result, we were able to delineate GTV_PCA (red line) excluding the draining veins. Graphically, the organ at risk 'vein' ROIs could be recognized as draining veins, and we confirmed the anatomical connection by referring to the DSA and IADCT images. Irradiation doses of 'vein' ROI were evidently reduced. Our method provides more accurate target delineation and reduction of wasteful operation time. Moreover, when larger AVMs are treated, this proposed method would be able to reduce the target volume dramatically, thereby allowing us to perform SRS more safely.

Since there are many types of AVMs (e.g., high flow, low flow, multiple feeders, etc.), we needed to analyze a sufficient amount of clinical data regarding the kind of cases that the PCA method could be adapted to clinically. One limitation is the substantial amount of time and work required for PCA data processing since this is currently performed virtually manually. In order to utilize this method for actual clinical treatment, it would be valuable to install the PCA method in a treatment planning workstation. In addition, in this study, a substantial amount of time was needed to acquire IADCT data because we used a dynamic study for each 3 mm interposi-

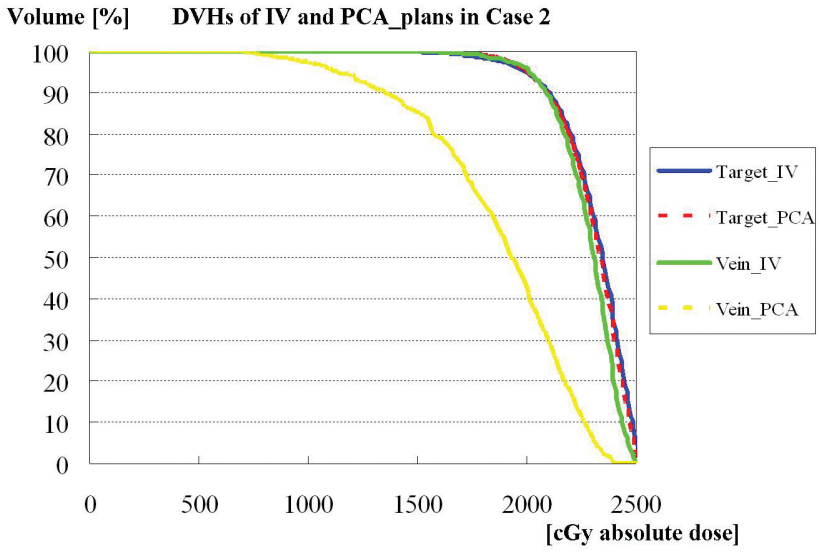

Fig. 7 Dose-volume histograms of IV and PCA_plans in Case 2.
Dose-volume histograms as absolute dose for the IV_plan (solid line) and PCA_plan (dotted line) are shown.

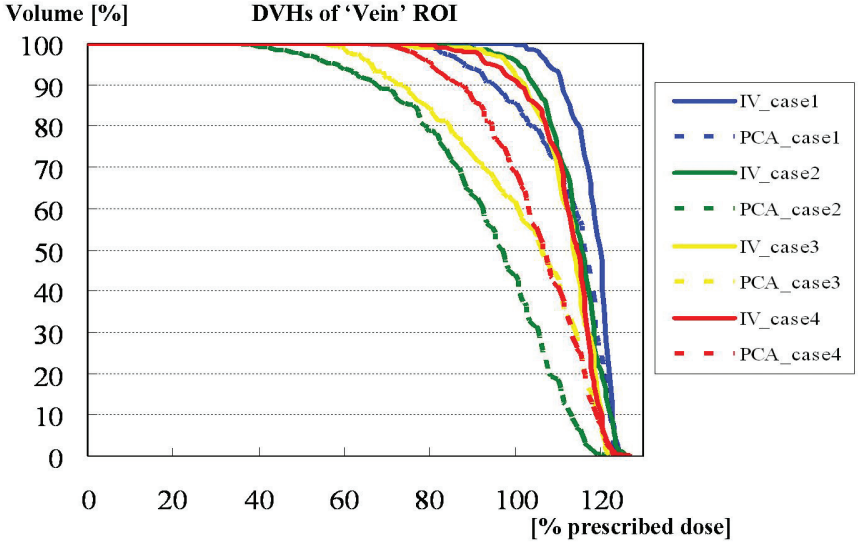

Fig. 8 Dose-volume histograms of the 'vein' ROI in Cases 1-4 for the IV_plan (solid line) and PCA_plan (dotted line).

tion slice with a single-row-detector. AVMs could be studied with IADCT in a very short time if 16- or 64-row multidetector CT (MDCT) was used; a practice that has become more widespread recently. The craniocaudal special resolution of MDCT-based IADCT is less than 0.6 mm. Our proposed method would be more practical using MDCT.

Conclusions

We proposed a novel method of extracting intracranial AVMs, and succeeded in accurately identifying the location of intracranial blood vessels by means of PCA. Furthermore, we were able to distinguish needless draining veins for radiosurgical targeting by using the principal component images. From these preliminary results, it was determined that there are some cases in which it is possible to make target delineation more accurate. In the

simulations, we were able to reduce the target volume using PCA images. The irradiation doses of these needless draining veins were also reduced. Further studies are needed to investigate the effectiveness of this method for other types of AVMs.

References

1. Pellettieri L, Svendsen P, Wikholm G, Carlsson CA: Hidden compartments in AVMs--a new concept. Acta Radiol 1997; **38**: 2–7
2. Lunsford LD, Kondziolka D, Flickinger JC: Stereotactic radiosurgery: current spectrum and results. Clin Neurosurg 1992; **38**: 405–444
3. Saunders WM, Winston KR, Siddon RL, Svensson GH, Kijewski PK, Rice RK, Hansen JL, Barth NH: Radiosurgery for arteriovenous malformations of the brain using a standard linear accelerator: rationale and technique. Int J Radiat Oncol Biol Phys 1988; **15**: 441–447
4. Awad IA, Magdinec M, Schubert A: Intracranial hypertension after resection of cerebral arteriovenous malformations. Predisposing factors and management strategy. Stroke 1994; **25**: 611–620
5. Pollock BE: Occlusive hyperemia: a radiosurgical phenomenon? Neurosurgery 2000; **47**: 1178–1182; discussion 1182–1174
6. Yeung D, Chen N, Ferguson RD, Lee LI, Kun LE: Three-dimensional reconstruction of arteriovenous malformations from multiple stereotactic angiograms. Med Phys 1996; **23**: 1797–1804
7. Tanaka H, Numaguchi Y, Konno S, Shrier DA, Shibata DK, Patel U: Initial experience with helical CT and 3D reconstruction in therapeutic planning of cerebral AVMs: comparison with 3D time-of-flight MRA and digital subtraction angiography. J Comput Assist Tomogr 1997; **21**: 811–817
8. Stancanello J, Cavedon C, Francescon P, Cerveri P, Ferrigno G, Colombo F, Perini S: Development and validation of a CT-3D rotational angiography registration method for AVM radiosurgery. Med Phys 2004; **31**: 1363–1371
9. Nyui Y, Ogawa K, Kunieda E, Kawaguchi O: Visualization of intracranial arteriovenous malformation using multivariate analysis. Nippon Igaku Hoshasen Gakkai Zasshi 2003; **63**: 322–328
10. Di Paola R, Bazin JP, Aubry F, Aurengo A, Cavailloles F, Herry JY, Kahn E: Handling of dynamic sequences in nuclear medicine. IEEE Trans Nucl Sci 1982; **29**: 1310–1321
11. Cavailloles F, Bazin JP, Di Paola R: Factor analysis in gated cardiac studies. J Nucl Med 1984; **25**: 1067–1079
12. Barber DC: The use of principal components in the quantitative analysis of gamma camera dynamic studies. Phys Med Biol 1980; **25**: 283–292
13. Knuttsson L, Bloch K, Holfas S, Wirestam R, Stahlberg F: Model-free arterial spin labelling for cerebral blood flow quantification: introduction of regional arterial input functions identified by factor analysis. Magn Reson Imaging 2008; **26**: 554–559
14. Eida S, Ohki M, Sumi M, Yamada T, Nakamura T: MR factor analysis: improved technology for the assessment of 2D dynamic structures of benign and malignant salivary gland tumors. J Magn Reson Imaging 2008; **27**: 1256–1262
15. Bucciolini M, Russo S, Banci Buonamici F, Pini S, Silli P: Dosimetric characterization of a bi-directional micromultileaf collimator for stereotactic applications. Med Phys 2002; **29**: 1456–1463
16. In: Schmidek HH, Roberts DW, eds, Schmidek & Sweet Operative Neurosurgical Techniques: Indications, Methods, and Results. 5th ed., Philadelphia, PA, Elsevier, 2006: 1269–1277.

Appendix

Details and principle of factor analysis for dynamic CT data set

We define the sequence of X-ray CT images as xij (k), where i and j are positions in the kth image (i = 1, … , n, j = =1, … , n). The total number of images is n.

Let xij (k) be the count of each pixel defined by the vector

$$\boldsymbol{X}ij = [xij(1), xij(2), \ldots, xij(k), \ldots, xij(n)] \quad (1)$$

represents the temporal evolution of the content of pixel (i, j). This elemental time-activity curve is called a "dixel" (pixel for dynamic studies). The entire information is contained in n×n dixels. Each pixel of an image corresponds to an underlying activity that is the summation of the activities of a number of anatomical components and physiological components. The kth image can be written as

$$xij(k) = aijA(k) + vijV(k) + mijM(k) + bijB(k) \quad (2)$$

where A(k), V(k), M(k), and B(k) represent the elementary activities corresponding to the arterial flow, the venous flow, the flow in nidus, and the background activity. The time-independent coefficients aij, vij, mij, and bij represent the contributions of each physiological component in the pixel (i, j). Bij(k) is the background component.

For each k the elementary activities A(k), V(k), M(k), and B(k) are non-negative, and coefficients aij, vij, mij, and bij are also non-negative.

The time evolution of a dixel (i, j) is

$$\boldsymbol{X}ij = aij\boldsymbol{A} + vij\boldsymbol{V} + mij\boldsymbol{M} + bij\boldsymbol{B} \quad (3)$$

where each vector is

$$\boldsymbol{A} = [A(1), A(2), \ldots, A(k), \ldots, A(p)] \quad (4)$$
$$\boldsymbol{V} = [V(1), V(2), \ldots, \mathrm{V}(k), \ldots, \mathrm{V}(p)] \quad (5)$$
$$\boldsymbol{M} = [M(1), M(2), \ldots, M(k), \ldots, M(p)] \quad (6)$$
$$\boldsymbol{B} = [B(1), B(2), \ldots, B(k), \ldots, B(p)] \quad (7)$$

These vectors represented as A, V, M, and B, are fundamental dynamic components, and vary with time. On the other hand, aij, vij, mij, and bij are coefficients that are independent of time.

The associated images composed of coefficients are called functional images, and are as follows:

$$\boldsymbol{I}a = aij \quad (8)$$
$$\boldsymbol{I}v = vij \quad (9)$$
$$\boldsymbol{I}m = mij \quad (10)$$
$$\boldsymbol{I}b = bij \quad (11)$$